INTERNATIONAL ATOMIC ENERGY AGENCY
UNITED NATIONS EDUCATIONAL, SCIENTIFIC AND CULTURAL ORGANIZATION

INTERNATIONAL CENTRE FOR THEORETICAL PHYSICS
34100 TRIESTE (ITALY) - P.O.B. 586 - MIRAMARE - STRADA COSTIERA 11 - TELEPHONE: 2240-1
CABLE: CENTRATOM - TELEX 460392 - I

SMR/206- 14

"SCHOOL ON POLYMER PHYSICS"

27 April - 15 May 1987

KEVLAR FIBRES

Profesor Abdelnour Michael HINDELEH
Department of Physics
University of Jordan
P.O. Box 13093
Amman, Jordan

Abstract

Kevlar fibres are aromatic polyamide fibres spun from the polymer poly(p-phenylene terephthalamide). Kelvar has a paracrystalline structure with less lattice distortion parameter in Kevlar 49 than in Kevlar 29. The equatorial X-ray "crystallinity" is 68% in Kevlar 29 and 76% in Kevlar 49. The fibres are classified as high-strength/high-modulus fibres. The small-angle X-ray diffraction pattern indicated that the Kevlar fibres have no chain folding. There is a statistical size distribution of microparacrystallites in the fibres. The melting point is over 500^{o}C .

Wide- and small-angle X-ray diffractior techniques, differential scanning calorimeter, differential thermal analysis, thermogravimetric analysis, transmission electron microscopy, scanning electron microscopy, and tensile testing equipment have been used to characterize the fibres and to assess the effect of annealing on their morphology and mechanical properties.

INTRODUCTION

The polymer poly(p-phenylene terephthalamide), abbreviated as PPT, was developed by E.I. Du Pont de Nemours & Co.[1,2], and spun into continuous non-twisted multifilament yarns of about 1500 Denier and containing e thousand filements per yarn. The trade names for PPT fibres are PRD49, Kevlar 49 and Kevlar 29. They are classified as high-strength/high-modulus fibres which are excellent for reinforcement in body armor and for fibre-reinforced composite materials for a host of applications including aerospace and vehicles industries, ropes and composites[3-8].

When Du Pont produced the PRD49 fibre they described it as "Aromatic Polyamide" [1,2]. The chemical composition of the fibre was characterized by Penn et. al.[9] who, after breaking down the fibre chemically, assigned equimolecular amounts of terephthalic acid and p-phenylene diamine as building blocks of the fibre. The currently accepted formula for PPT fibres, as suggested by Carter and Schenk [10] is poly(p-phenylene terephthalamide):

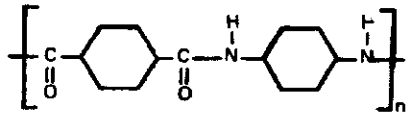

On the basis of the wide-angle X-ray diffraction analysis of the polymer poly(p-phenylene terephthalamide), prepared and spun into fibres in the laboratory, Northolt et. al. [11-13] assigned a monoclinic (pseudo-orthorhombic) unit cell with dimensions a=7.87 Å, b=5.18 Å, c(fibre axis) = 12.9 Å, and $\gamma = 90^{\circ}$. The unit cell contains two chains as shown in Figure 1. The chains are linked together by hydrogen bonds, and form crystalline domains. Due to the intramolecular interactions between sequential phenyl and amide segments in the chain, Northolt [13] assumes that free rotation around the phenyl-carbonyl and the phenyl-

nitrogen bonds is absent. Consequently the chains are regarded as a rigid rod. Such a structure has a considerable bearing on the tensile properties of Kevlar fibres which possess a high modulus.

The present paper will tackle the morphology of the PPT fibres, examined by wide- and small-angle X-ray diffraction techniques, transmission and scanning electron microscopy, thermal analysis (TGA, DSC and DTA), tensile properties, the effect of annealing and thermal ageing on the morphology and properties, and the fields of application of these fibres.

EXPERIMENTAL

X-Ray Diffraction

Wide- and small-angle X-ray diffraction studies included the following parameters:

(a) The lattice distortion parameter (g).
(b) The crystallinity.
(c) The microparacrystal (mPC) size.
(d) The orientation.
(e) Chain folding.
(f) Voids.

Two wide-angle X-ray diffraction techniques have been used, namely the photographic and the diffractometric. A bundle of parallel filaments was exposed to CuK_α X-ray with the beam being perpendicular to the fibre axis. The diffraction pattern was recorded in a Searle camera fitted with Elliot toroidal mirror optics [14] and a cylindrical cassette of 3 cm radius. The specimen to film distance for the wide-angle pattern was 3 cm, and for the small-angle pattern 30 cm. For the determination of the crystallinity and mPC size a flat bundle of the fibres was

mounted on a special flat holder in a Philips diffractometer PW1050. To eliminate the effect of orientation on the measurement of crystallinity, the sample holder was rotated at a speed of 80 r.p.m. The equatorial intensity was scanned either in the continuous-mode or in the step-scan mode in steps of $0.1^{\circ}(2\theta)$ and a counting time of 10 sec., thus obtaining a print-out of intensity against 2θ. For the determination of the Orientation, a bundle of parallel fibres was mounted in a Philips Norelco X-ray diffractometer operated in the transmission mode. The azimuthal intensities of the (200) reflection on both sides of the diffraction pattern was recorded.

The Lattice Distortion Parameter (g)

Hosemann and his colleagues introduced and promulgated in over 250 publications the concept of "Paracrystallinity" in polymers. The concept implies that the crystallites in polymers, as well as in many other materials, have never attained the ideal state of a perfect lattice, but they contain distortions which put them into a category called "Paracrystals". Hosemann showed how simple point lattice masks could be used in an optical diffractometer to illustrate the idea of short-range disorder, which gives rise to the so-called distortion of the first kind, and of long-range disorder, which gives rise to distortion of the second kin. Distortion of the first kind causes a reduction in height of successive diffraction peaks without change in breadth, whereas distortion of the second kind causes an increase in breadth together with a reduction in amplitude [15-22]. Hindeleh and Johnson[23] prepared a series of masks with 100 lattice layers containing distortion of the second kind ranging between 0 and 10% and obtained optical transforms for them, and showed that the increase in distortion yields diffraction profiles with greater width and smaller amplitude (see Figure 2).)

Figure 3 shows a computer-constructed two-dimensional paracrystalline lattice[19,21]. With a growing lattice the statistical fluctuations finally becomes so large to the extent

that the binding angles of the atoms are over-strained and the net-plane breaks (see arrow in Figure 3). The diffraction pattern of this model shows an increase in the integral breadth (δb) of the reflections proportional to the square of the order of reflection (ℓ), typical of the diffraction pattern of real polymers. When a curve is drawn between δb and ℓ^2, the intercept of the curve with the ordinate gives the size of the microparacrystal $\overline{D}$ and the number of layer lines ($\overline{N} = \overline{D} / \overline{d}$) where $\overline{d}$ is the mean net-plane distance. From the slope of the curve, the distortion parameter (g), which represents the statistical fluctuation of the net-plane distances, is calculated according to Hosemann's equation:

$$\delta b = \frac{1}{\overline{D}} - \frac{(\pi g)^2}{\overline{d}} \ell^2 \quad \ldots\ldots\ldots\ldots\ldots\ldots\ldots \quad 1$$

Crystallinity

The intensity data obtained from the diffractometeric equatorial equatorial scan of the wide-angle x-ray diffraction pattern was then corrected for air scatter, polarization, Compton scatter and Lorentz factor, and finally normalizec to a convenient area under the scan. The scan contairs overlapping peaks which represent the scatter from the hkl planes and a background scatter (anisotropic scatter). Resolution of the peaks and background was achieved by the "Multipeak Resolution" program developed by Hindeleh and Johnson, and applied to the X-ray investigation of natural and synthetic polymers [24-26].

Each peak is mathematically fittec into a combined Gaussian/ Cauchy profile in the form:

$$f_t G_t + (1 - f_t) C_t \quad \ldots\ldots\ldots\ldots\ldots\ldots \quad 2$$

where f is the Gaussian fraction, and t is the hkl-plane peak number 1,2,3....B. B represents the number of peaks to be resolved. f is called the "profile-function parameter".

The Gaussian function G_t is $$A_t \exp\left\{-\ln 2\left[\frac{2(X - P_t)}{W_t}\right]^2\right\} \quad \ldots\ldots\ldots\ldots 3$$

and the Cauchy function C_t is $$A_t / \left\{1 + \left[2(X - P_t)/W_t\right]^2\right\} \quad \ldots\ldots\ldots\ldots 4$$

Thus each peak is defined by four quantities: A, the amplitude of the peak, W the width of the peak at 50% amplitude, P the peak position on the 2θ scale, and f the profile-function parameter which takes values between -0.5 and 1.0. For a Gaussian profile f=1, for a Cauchy profile f=0, for a combined Gaussian/Cauchy profile ($-0.5 < f < 1$); f effectively describes the tail of the profile as shown in Figure 4 . The background scatter is assigned a polynomial equatior of the form:

$$R = a + bX + cX^2 + dX^3 \quad \ldots\ldots\ldots\ldots 5$$

where X is the 2θ scale, and a,b,c, and d are adjustable parameters.

At the beginning of resolution, the parameters for each peak and the parameters of the background are assigned approximate values. The resolution program incorporates an iterative minimization procedure based on Powell's method of conjugate directions(27)) which ensures efficient convergence of the factor factor S:

$$S = \sum_{i=1}^{n}\left[I_{(calc)_i} - I_{(norm)_i}\right]^2 \quad \ldots\ldots\ldots\ldots 6$$

where

$$I_{(calc)_i} = \sum_{t=1}^{B}\left[f_t G_t + (1 - f_t)C_t\right]_i + R_i \quad \ldots\ldots\ldots\ldots 7$$

Here, n is an array of data points of 2θ versus I, and B is the number of peaks.

The "Peak Area Crystallinity" is then a parameter defined as the ratio of the scatter under the resolved peaks to the total scatter under the normalized X-ray diffraction scan.

Microparacrystallite (mPC) Size

The resolved peaks were then corrected for instrumental broadening using Stoke's deconvolution method[28] and hexamethylene tetramine as standard[25]. The integral breadth d(2θ) of the corrected peak profile was used to calculate the mPC size $\bar{L}_{hkl}$ normal to a set of hkl netplanes according to Scherrer's equation:

$$\bar{L}_{hkl} = \frac{1}{\delta(2\theta)} = \frac{K\lambda}{\cos\theta \, \delta(2\theta)} \qquad \ldots\ldots\ldots\ldots\ldots\ldots\ldots\ldots \quad 8$$

where K is a const ≈ 1, and $\delta(2\theta)$ is obtained from the area under the resolved peak divided by its amplitude, $\delta(2\theta)$ is expressed in radians.

Microparacrystallite Orientation

The microparacrystallite orientation in Kevlar fibres was determined from the WAXS pattern. A bundle of parallel fibres was mounted in a Philips Norelco X-ray diffractometer operated in the transmission mode. The azimuthal intensities of the (200) reflection on both sides of the diffraction pattern were recorded. The orientation parameters $\langle \sin^2 \psi_{h00} \rangle$ was evaluated from the azimuthal-intensity data according to Stein's equation[29]

$$\langle \sin^2 \psi_{h00} \rangle = \frac{\int_0^{\pi/2} I(\psi_{h00}) \sin^2 \psi_{h00} \cos\psi_{h00} \, d\psi_{h00}}{\int_0^{\pi/2} I(\psi_{h00}) \cos\psi_{h00} \, d\psi_{h00}} \qquad \ldots\ldots\ldots\ldots\ldots \quad 9$$

where $I(\psi_{h00})$ is the intensity distribution, and ψ_{h00} is the azimuthal angle measured from the equator.

RESULTS

Wide-Angle X-ray Diffraction (WAXS) Pattern

Figure 5 shows the WAXS pattern of Kevlar fibres. The principal diffraction maxima are the innermost equatorial reflections (110) and (200), and the meridional reflections (002), (004) and (006). The netplanes spacings are: $\overline{d}_{110}$ = 0.431 nm, $\overline{d}_{200}$ = 0.385 nm, $\overline{d}_{002}$ = 0.645 nm, $\overline{d}_{004}$ = 0.320 nm, and $\overline{c}_{006}$ = 0.213nm.

The WAXS pattern persisted until an annealing temperature of 450°C in Kevlar 29 and 500°C in Kevlar 49. After these temperatures the pattern lost its identity [32,33].

Small-Angle X-Ray Diffraction (SAXS) Pattern

Figure 6 shows the SAXS pattern of Kevlar 29 fibres [32] at all temperature levels up to 400°C. It consists of an equatorial streak resembling the patterns obtained from the other PPT fibres specimens[13,35-37]. This pattern implies the presence of needle-like voids with the larger axis lying parallel to the fibre axis[36,37]. The absence of meridional reflections, which are traditionally associated with chain folding in polyamide and polyester fibres, indicates that Kevlar fibres have no chain folding, and supports the concept of the rigid rod-like structure of the Kevlar molecular chains.

Orientation

The azimuthal intensity profiles of Kevlar 29 and Kevlar 49 are illustrated in Figure 7. The values of the profile width at half-maximum height and the orientation parameter $\langle \sin^2 \psi_{200} \rangle$ of several Kevlar fibres are given in Table 1.

Table 1: The Orientation Parameter of Kevlar Fibres

Type of Fibre	Profile Width at half-Maximum height (degree)	Orientation Parameter $\langle \sin^2 \psi_{zcc} \rangle$	Ref.
Kevlar 29	18.9	0.047	32
Kevlar 49	12.4	0.020	33
Model Samples		0.016 - 0.048	34

It is concluded, from Table 1, that Kevlar 49 is better oriented than Kevlar 29. Compared with many other textile fibres, the two types of Kevlar fibres are very well oriented.

Lattice-Distortion Parameter (g)

Figure 8 shows a plot of the integral breadth (β_b) of the reflections (002), (004), and (006) of the Kevlar 29 fibre against the square of the order (ℓ). It shows that β_b increases quadratically with higher orders of reflection. From the intercept of the curve with the ordinate the mPC size $\overline{D}_{002}$ was determined. The lattice distortion parameter (g) was calculated according to equation 1. A comparison of the average mPC size $\overline{D}_{002}$, the average number $\overline{N}_{002}$ of netplane layers, and the lattice-distortion parameter (g) of different PPT fibres is given in Table 2.

The product of (g) and the $\overline{N}$ is an empirical parameter, called α^* constant, introduced by Hosemann for paracrystalline materials:

$$\alpha^* = \sqrt{\overline{N}}\, g = \sqrt{\overline{D}/d} = 0.1 \text{ to } 0.2 \quad \ldots\ldots\ldots \quad 10$$

In his extensive work on different materials, Hosemann found that α^* ranges between 0.1 and 0.2. The physical implication of α^* is that there is a limit to the growth of mPCs controlled by (g), as has been mentioned in connection with Figure 3 [21]. Table 2 indicates that for PRD 49, $\alpha^* = 0.16$, and for the other model PPT fibres, $\alpha^* = 0.18$. These values fit well into Hosemann's assembly of paracrystalline materials [21] as shown in Figure 9.

The untreated Kevlar 29 has an extraordinary value of α^* due to its high (g) value. However, after annealing at temperatures between 100° and 400°C for 15 min. α^* decreased to the range 0.22-0.25. Here it is remarkable that even after annealing the fibre Kevlar 29, g does not recover completely to the normal value of the other PPT fibres listed in Table 2. Therefore, the distortions remained anchored within the lattice. The slow decrease of α^* after annealing could be explained by the fact that the Kevlar 29 was not in an equilibrium state when initially produced[22].

Table 2

A Comparison between $\bar{D}_{002}$, $\bar{N}_{002}$, g and α^* - value of PPT fibres.

Fibre	$\bar{D}_{002}$ (nm)	$\bar{N}_{002}$	g	Ref.	α^*
Untreated					
PRD 49	38	59	0.021	21,35	0.16
Kevlar 49			0.015	31	
Kevlar 29	50	76	0.059	32	0.51
Other models	70	108	0.017	13	0.18
Annealed Kevlar 29				32	
100°C, 15 min.	14.3	22	0.047		0.22
300°C, 15 min.	14.9	23	0.046		0.22
350°C, 15 min.	15.2	24	0.050		0.24
400°C, 15 min.	14.7	23	0.052		0.25
300°C, 2hr.	16.1	25	0.046		0.23
4hr.	16.1	25	0.049		0.24
46	17.0	26	0.054		0.28

Crystallinity

Figure 10 shows the equatorial X-ray diffraction scan in the range 10 to 30° (2θ). After 30°, the scan becomes flat. Each scan has been resolved into two peaks (110) and (200) and a background. Figure 11 compares the equatorial scans of Kevlar 29 and Kevlar 49 at 500°C, and shows clearly how the diffraction pattern of Kevlar 29 vanishes at 500°c, while that of Kevlar 49 persists.

A comparison between the crystallinities of Kevlar 29 and Kevlar 49 is shown in Figure 12.[32,33]. The crystallinity of the untreated Kevlar 29 was 68%, and increased gradually with increasing the annealing temperature. Between 300°C and 400°C the crystallinity reached a plateau region of 75% crystallinity. At 450°C the crystallinity decreased to 60% and at 500°C the diffraction pattern vanished as was shown above in Figure 11. On the other hand, the untreated Kevlar 49 had a crystallinity of 76% which remained constant in the samples that had been annealed until 350°C. At 400°C the crystallinity reached its maximum value 81%. At 450°C the crystallinity decreased to 64%, and at 500°C it decreased to 51%.

Microparacrystallite Size

A comparison of the mPC sizes $\overline{D}_{110}$ and $\overline{D}_{200}$ of Kevlar 29 and Kevlar 49 is shown in Figure 13.[32,33]. The untreated Kevlar 29 had $\overline{D}_{110}$ = 4.37 nm and $\overline{D}_{200}$= 3.56 nm. The untreated Kevlar 49 had $\overline{D}_{110}$ = 4.25 nm and $\overline{D}_{200}$= 3.83 nm. In both fibres, the mPC sizes remained almost unchanged until 150°C, after which the rate of increase in mPC sizes of Kevlar 29 has been more remarkable than in Kevlar 49. For both fibres, the maximum sizes were attained at 400°C when $\overline{D}_{110}$ reached 6.28 nm and $\overline{D}_{200}$= 4.51 nm for Kevlar 29, while for Kevlar 49 $\overline{D}_{110}$ reached 4.89 nm and $\overline{D}_{200}$ = 4.27 nm. After 450°C the mPC sizes decreased in both fibres as shown in Figure 13.

Effect of Thermal Ageing on the Crystallinity of Kevlar 49

Figure 14 shows the crystallinity as a function of ageing time in air at 150°C of Kevlar 49 fibres. Up to 4 days no change in crystallinity occured. After 4 days a drop in crystallinity from 74,8 to 71.5 % occured. Between 8 days and 16 days the crystallinity maintained the same value (~ 71%). After 16 days the decrease in crystallinity was slow and gradual. After 44 days the crystallinity became 62.3 % and remained constant until 120 days.

Effect of Thermal Ageing on the Crystallite Size of Kevlar 49

A slight gradual increese in size occured as a result of thermal ageing below 32 days. For example, $\bar{D}_{110}$ was 4.29 nm for the untreated fibre and reached the maximum value 5.20 nm after 32 days of ageing, after which the size decreased gradually, thus reaching a value of 4.12 after 120 days.

THERMAL ANALYSIS

Thermogravimetric analysis:

The humidity in Kevlar 29 and Kevlar 49 fibres, dried at 105°C in vacuum, is 3.5% and 2.8% respectively. The oven-dry weight was then regarded as reference for subsequent determination of weight-loss at higher temperatures. Figure 16 shows the weight loss against g temperature in nitrogen atmosphere in the temperature range 100-700°C. Up to 300°C there is practically a plateau region of negligible loss in weight in both types of fibres. At 350°C the loss was only 1%; at 400°C the weight-loss in Kevlar 29 amounted to 2.9% and in Kevlar 49, 2.2%. After 400°C the rate of weight-loss became higher in Kevlar 29; and at 675°C the loss amounted ito 51% in Kevlar 29 and 20% in Kevlar 49.

Melting Point

Figure 17 shows a DSC curve of Kevlar 29. The change in the slope of the curve after 450°C implies that melting started at about 500 C which is concurrent with the phenomenon of diffuse X-ray diffraction pattern at this stemperature (see the equatorial scan in Figure 8c). The peak melting point is 600°C; this value is much higher than the melting points of many organic polymers (39). Although the melting point of a polymer is generally reported as a single temperature at which the transition from the solid phase to the liquid phase is complete, fusion can spread over a range of temperature due to distribution in mPC size (21,31,40,41). The wide spread in the mPC size in Kevlar fibres has been mentioned on page /4. Compared with the DSC curves of PE and PP, the melting poofile of Kevlar 29 is broad (42,43).

Figure 18 shows a DTA curve of Kevlar 49 fibre. The peak melting point for the untreated fibre is 536.7°C. When the fibre was annealed at 150°C, the melting point increased to 540°C, and when the fibre was annealed at 200°C, the melting point became 541.3°C.

ELECTRON MICROSCOPY

Transmission Electron Microscope (TEM)

The first successful electron-microscope photograph showing the lattice images in an organic polymer was published by Dobb, et. al. (30) (see Figure 15). The photograph showed the long chain molecules in Kevlar 49 fibres. Individual layers of molecules spaced 0.433 nm apart could be seen clearly and the size of the units in which they pack together could be measured directly from the photograph. Although similar lattice images were recorded before, for example, in carbon fibres (38), organic fibres are usually far too sensitive to the electron beam in the microscope and are destroyed before pictures can be recorded. The Kevlar 49 pictures were taken in a Philips EM300 operated at 100 KV with an anticontamination trap, under a high-resolution condition. The EM photographs revealed that Kevlar 49 chain molecules are long, straight, and packed together regularly with very little distortion, the prerequisites for ultra high modulus and tensile strength (45,46)

Dobb et. al.[31] demonstrated further how the lattice from the (110) and (002) netplanes of Kevlar fibres is in the form of arrays of almost parallel fringes, but in rare cases slightly curved lattices were observed. They also reported a statistical distribution of the microparacrystal size in PRD 49 and Kevlar 49 obtained by counting the lattice fringes from the (110) netplane layers of 500 microparacrystals. The number of lattice fringes in PRD 49 ranged between 4 and 24 fringes with $\overline{N}_{110}$ = 12 corresponding to an average size $\overline{D}_{110}$ of 5.4 nm. In Kevlar 49, $\overline{N}_{110}$=11 and $\overline{D}_{110}$ =4.9 nm. The EM studies were also supplemented by X-Ray diffraction.

The size distribution of microparacrystals mentioned above is in agreement with the theoretical predictions of Hosemann et. al.[21,47] for $\overline{N}$=11.

Scanning Electron-Microscopy (SEM)

The SEM micrographs showed that the surface of Kevlar fibres is smooth, but after annealing some roughness started to appear on the surface, which could be attributed to the attempt of trapped vapor to escape.

The loop test was performed to study the occurrence of cracks or kinks in compression. Slides will be displayed during the lecture which will show the following: (a) macrofibrils of 300 nm diameter, (b) the surface of the fibres before and after annealing, (c) the splitting of the fibre into layers, and (d) the occurence of kinks and cracks due to compression during the "elastic loop" test.

MECHANICAL PROPERTIES

The untreated Kevlar 29 and Kevlar 49 fibres have high tensile strength of 2.81 GNm^{-2}, that is greater than the tensile strength of the widely-used polyamide and polyester fibres, and close to the tensile strength of steel, boron, or carbon fibres as shown in Table 3. The strain at break of Kevlar 29 is 3.8 %, by far lower thank that of the polyamide and polyester fibres, but higher than the strain at break of steel, boron or carbon fibres. The strain at break of Kevlar 49 is 2.4 %, close to that of steel. The stress-strain curve of Kevlar fibres is illustrated in Figure 19 which indicates that the Young's modulus is constant up to high stresses and amounts to 63 GNm^{-2} in Kevlar 29 and 113 GNm^{-2} in Kevlar 49. This behaviour can be attributed to characteristic structural features among which are the following:

(a) The rigid rod-like molecular chain,
(b) the cohesion between the chains which is enhanced by the hydrogen-bonding,
(c) the high crystallinity,
(d) the good mPC orientation relative to the fibre axis, especially in Kevlar 49.

Table 3

Comparison of the Mechanical Properties of Some Polymers

Polymer	Tensile Strength (GNm^{-2})	Strain at break (%)	Young's Modulus (GNm^{-2})	Ref.
Kevlar 29	2.8	3.8	63.1	32
Kevlar 49	2.8	2.4	113.0	33
Nylon(high-strength)	1.0	17.0	12.5	44
Polyester(high-strength)	1.0	20.0	18.5	44
Steel	2.0	2.0	200.0	44
Boron	3.5	1.5	370.0	44
Carbon HS	2.0	0.8	270.0	44

The annealing effects on the mechanical properties of Kevlar 29 have been studie in detail [32]. Neither the tensile strength nor the strain at break showed an appreciable change upon annealing at temperatures below 200°C in Nitrogen gas, as shown in Figure 20. However, a significant decrease in tensile strength and strain at break occurred at elevated temperatures. Figure 20 shows the tensile strength, strain at break and Young's modulus as functions of the annealing temperature. The Young's modulus increased with the increase in annealing temperature up to 300°C. This is concurrent with the increase in the crystallinity and mPC sizes. The decrease in the modulus at temperature higher than 300°C could be attributed to the lateral melting of smaller mPCs.

Prolonged annealing at 300°C caused further drop in the tensile strength and strain at break and modulus, as shown in Table 4. The effect on the modulus is smaller than what would be expected from an organic polymer heat-treated uner these conditions.

Table 4

Effect of Prolonged Annealing at 300°C in Nitrogen Gas on the Mechanical Properties of Kevlar 29 (32)

Treatment	Tensile Strength (GNm^{-2})	Strain at Break (%)	Young's Modulus (GNm^{-2})
Untreated	2.81	3.80	63.9
300°C, 15 min	2.50	2.85	79.0
2 hours	2.0C	2.80	73.5
4 hours	1.96	2.70	73.7
16 hours	1.22	1.91	73.2
46 hours	1.02	1.70	68.0

REFERENCES

1. E. I. Du Pont de Nemours & Co., U.S.Pat. 3,869, 430; Brit. Pat. 1, 391, 501

2. Chem. Eng. New, 50, 33 (1972).

3. J. Preston, Polymer. Eng. Sc., 15(3), 199 (1975).

4. A. R. Bunsell, J. Mat Sci., 10, 1300 (1975).

5. T. T. Chiao and R. L. Moore, Composites, 7, 31 (1973).

6. J. W. Moore and D. L. Sturgeon, Composites, 7, 34 (1973).

7. P. L. Walton and A. J. Majudar, J. Mat. Sci., 13, 1075 (1978).

8. R. E. Allred, J. Composite Materials, 15, 100 (1981) and 15, 117 (1981).

9. L. Penn, H. A. Newey and T. T. Chiao, J. Mat. Sci. (Letters), 11, 190 (1976).

10. G. B. Carter and V. T. J Schenk, Physics Bulletin 24, 716 (1973).

11. M. G. Northolt and J. J. Van Aartsen, J. Polymer. Sci., Polym. Lett. Ed. 11, 333 (1973).

12. M. G. Northelt, European Polymer J., 10 , 799 (1974).

13. M. G. Northolt and J. J. Van Aartsen, J. Polymer Sci. (Pol. Symp.), 58, 238 (1977).

14. A. Elliott, J. Sci. Instrum., 42, 312 (1967).

15. R. Hosemann,and S.N.Bagchi,"Direct Analysis of Diffraction by Matter", North Holland Publishing Co., Amsterdam, 1962.

16. R. Hosemann, J. Appl. Phys., 34, 25 (1963).

17. R. Hosemann, K. Lemm, A. Schonfeld, and W. Wilke, Kolloid-Z. Polym., 103, 216 (1967).

18. R. Hosemann and W. Wilke, Makromol. Chem., 118, 230 (1966).

19. F. J. Balta-Calleja and R. Hosemann, J. Appl. Crystallogr. 13, 521 (1980).

20. R. Hosemann, W. Vogel and D. Weick, Acta Crystallogr., A37, 85 (1981).

21. A. M. Hindeleh and R. Hosemann, Polymer (Polym. Comm.), 23, 1101 (1982).

22. R. Hosemann, M. P. Hentschell, F. J. Balta'-Calleja, E. Lopez Cabarcos and A. M. Hindeleh. J. Phys. C: Solid State Phys., 18, 961 (1985).

23. A. M. Hindeleh and D. J. Johnson, Polymer, 21, 929 (1980).

24. A. M. Hindeleh and D. J. Johsnon, J. Phys. D.: Appl. Phys., 4, 259 (1971).

25. A. M. Hindeleh and D. J. Johnson, Polymer,
(a) 13, 27 (1972); (b) 13,423 (1972);
(c) 15, 697 (1974); (d) 19, 27 (1978);

26. A. M. Hindeleh, D. J. Johnson, and P. E. Montague, Computational Methods for Profile Resolution and Crystallite Size Evaluation in Fibrous Polymers, in "Fiber Diffraction Methods", ACS Symp., Ser. No. 141. 1980, pp. 149-182.

27. M. J. D. Powell, Comput. J., 7, 155 (1964).

28. A. R. Stokes, Proc. Phys. Soc., A61, 382 (1948).

29. R. S. Stein, J. Polym. Sci., 31, 327 (1958).

30. M. G. Dobb, A. M. Hindeleh, D. J. Johnson and B. P. Saville, Nature, 253, 189 (1975).

31. M. G. Dobb, D. J. Johnson, and B. P. Saville, J. Polymer Sci., Polym. Symp. 58, 237 (1977).

32. A. M. Hindeleh, N. A. Halim and K. A. Ziq, J. Macromol. Sci. - Phys., B23 (3),289 (1984).

33. A. M. Hindeleh and Sh. Abdo, in publication.

34. M. G. Northolt, Polymer, 21, 1199 (1980).

35. A. M. Hindeleh, J. Haase, J.Capo, and G.S.Y.Yeh, in publication.

36. A. Majeed, Ph.D. Thesis, University of Leeds, 1978.

37. M. G. Dobb, D. J. Johnson, A. Majeed, and B. P. Saville, Polymer, 20, 1284 (1979).

38. D. Grawford, and D. J. Johnson, J. Microsco., 94, Pt.1, 51 (1971).

39. L. Mandelkern, "An Introduction to Macromolecules", Springer-verlag, New York, 1972, P.83.

40. W. P. Brennan, "Characterization of Polyethylene Films by Differential Scanning Calorimetry". Bull. No. 24, Perkin Elmer Corporation Instrumental Division, March 1978.

41. G. S. Y. Yeh, R. Hosemann, J. Lobode-Čačkovic´, and H. Čačkovic', Polymer, 17, 309)1976).

42. A. M. Hindeleh and N. S. Breik, in publication

43. M. A. Issa, Ph. D. Thesis, University of Jordan, 1983.

44. M. H. Lafitte and A. R. Bunsell, J. Mat. Sci., 17,2391(1982).

45. G. B. Carter and V. T. J. Schenk, "The Structure and Properties of Oriented Polymers", I. M. Ward, Ed., Applied Science, London, 1975, Ch. 15.

46. M. P. Hentschel and A. Lange, BAM Internal Report, W. Berlin, 16, 3, 310(1986).

47. R. Hosemann, W. Schmidt, A. Lange and M. Hentschel, Colloid & Polymer Sci., 259, 1161 (1981)

FIGURE CAPTIONS

Figure 1: Unit cell of the polymer poly (p-phenylene terephthalamide).

2: First-order Profile of computer-drawn two-dimensional paracrystals with N = 100 and 0, 4, 8, 10% distortions.

3: Computer-drawn two-dimensional Paracrystal with g = 0.02 and N = 49 similar to g for PPT fibres. The arrow indicates the breakdown of the constructuon.

4: Profile-function parameter f :
(A) Gaussian f=1 (B) Cauchy f = 0
(C) Combined Gaussian/Cauchy f = 0.5
(D) Combined Gaussian/Cauchy f = -0.5

5: Wide angle X-ray scattering of Kevlar 29.

6: Small-angle X-ray Scattering of Kevlar 29.

7: Azimuthal intensity profile of the (200) reflection of Kevlar 29.

8: The $\hat{a}\, b\text{-}\ell^2$ plot of the reflections (002), (004), and (006) of Kevlar 29 annealed for 15 min. at 300°C

9: Hosemann's collection of materials with $\alpha^* = 0.1$ to 0.2. PPT fibres are included: + PRD49 ■ Kevlar 29 at 300 C°.

10: Equatorial X-ray diffraction scan of Kevlar 29 resolved into two peaks and background.

11: Equatorial X-ray diffraction scans of Kevlar 29 and Kevlar 49 annealed at 500°C.

12: Crystallinity of Kevlar 29 and Kevlar 49 annealed in N_2 gas in the temperature range 20-500°C.

Finure 13: Microparacrystallite sizes $\bar{D}_{110}$ and $\bar{D}_{200}$ of Kevlar 29 and Kevlar 49 annealed in N_2 gas in the temperature range 20-500°C.

14: Effect of ageing at 150°C in air for periods ranging from 1 to 120 days.

15: Electron micrograph of the lattice fringes in Kevlar 49.

16: Thermogravimetric analysis of Kevlar 29 and Kevlar 49 in N_2 gas in the temperature range 20-700°C.

17: DSC curve of Kevlar 29.

18: TGA and DTA curves of Kevlar 49.

19: Stress-Strain curve of Kevlar 29.

20: Tensile strengh, Breaking strain and Young's Modulus of Kevlar 29 annealed in gas in the temperature range 20-400°C.

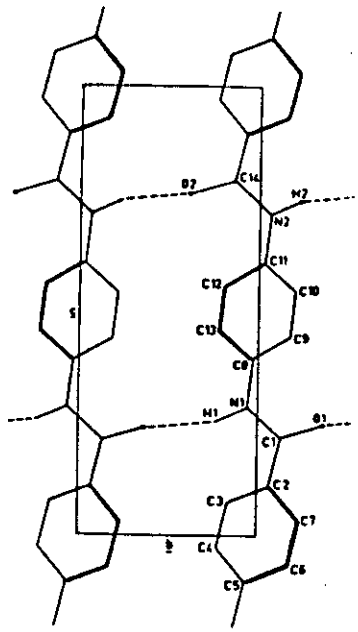

Figure 1

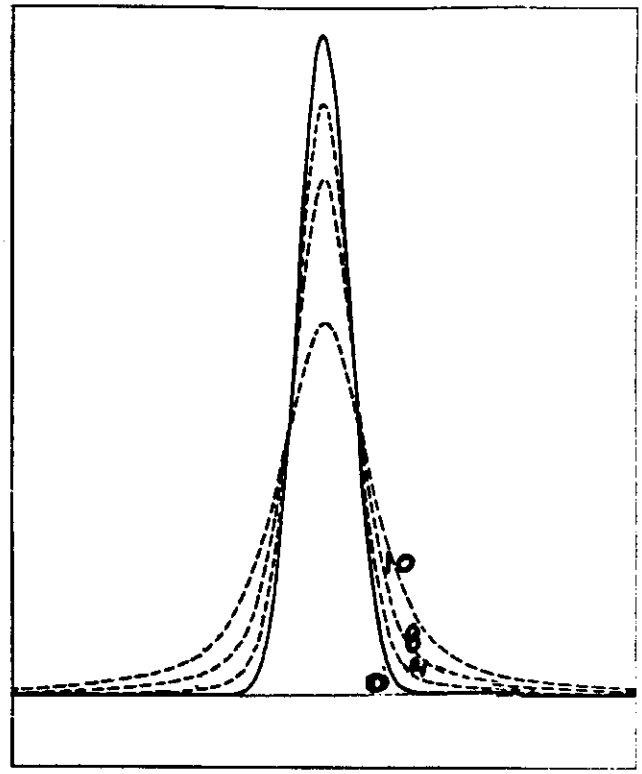

Figure 2

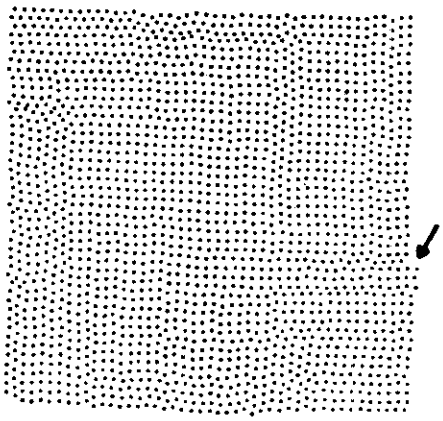

Figure 3

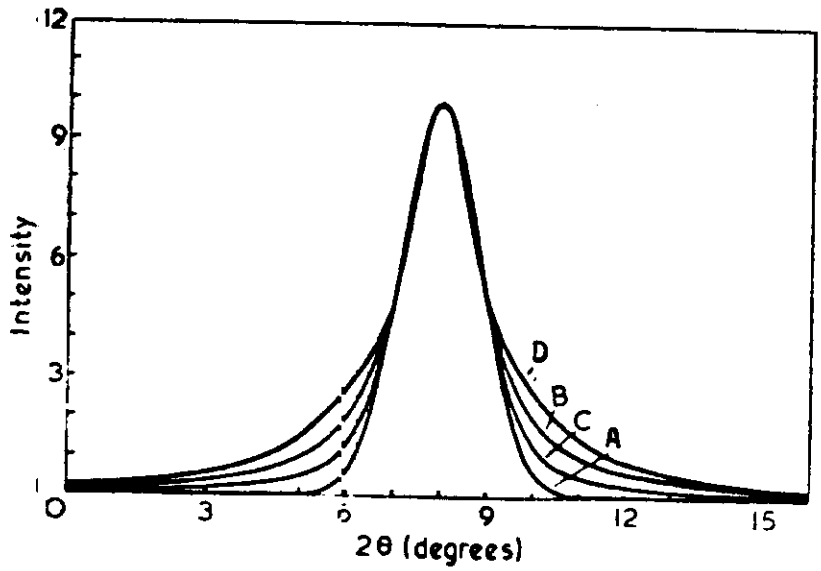

Figure 4

Figure 5

Figure 6

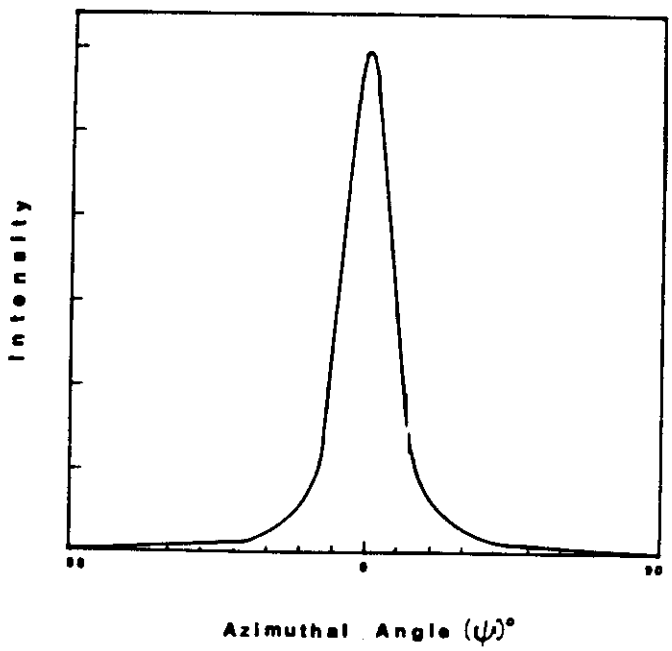

Figure 7

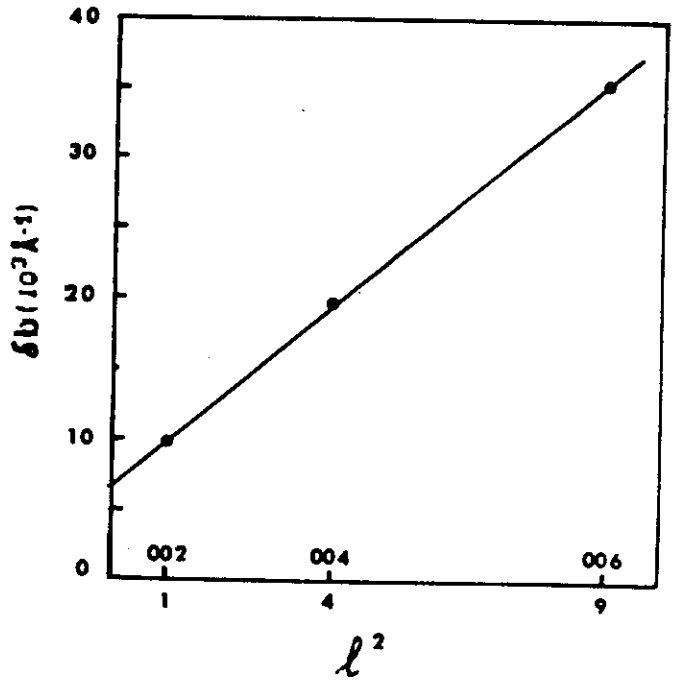

Figure 8

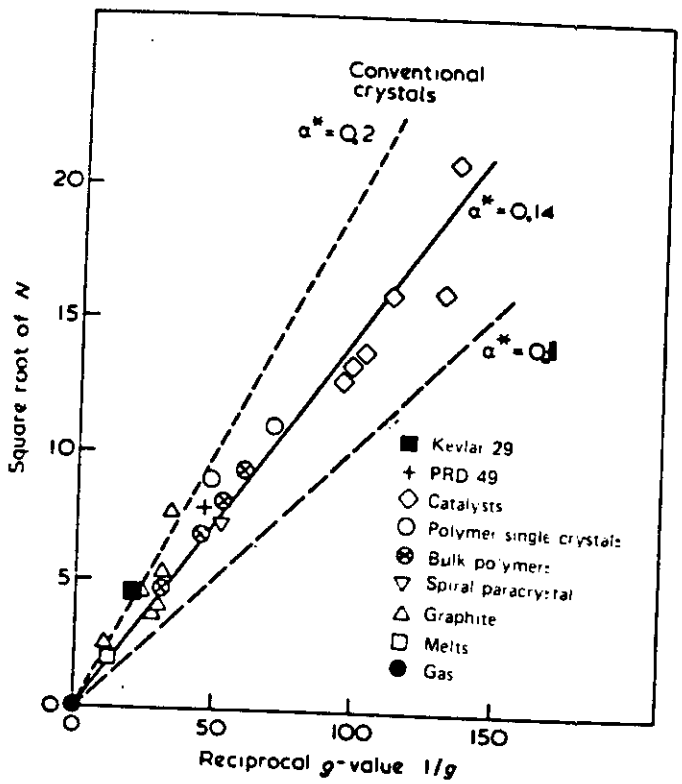

Figure 9

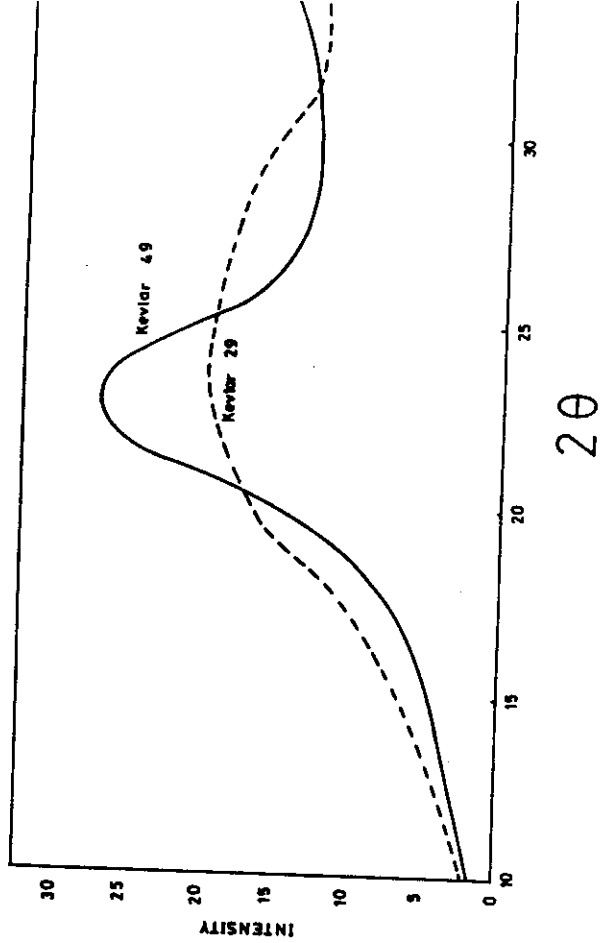

Figure 11

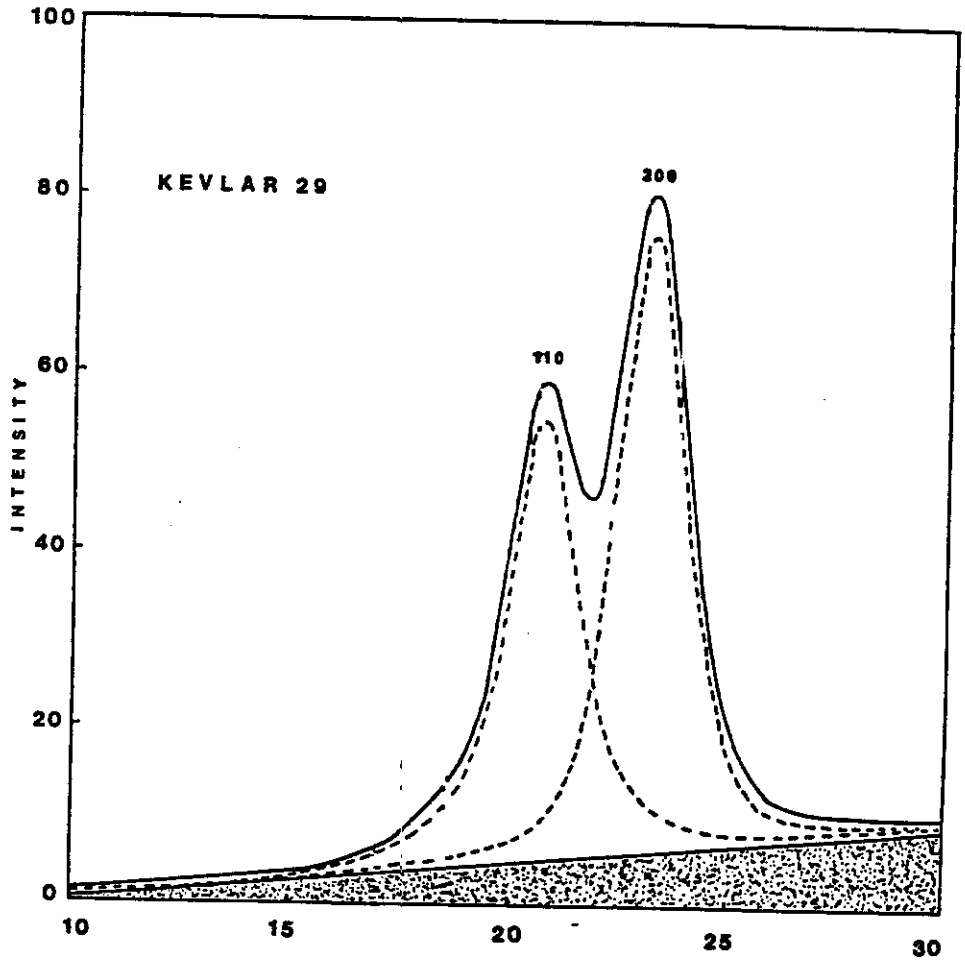

Figure 10

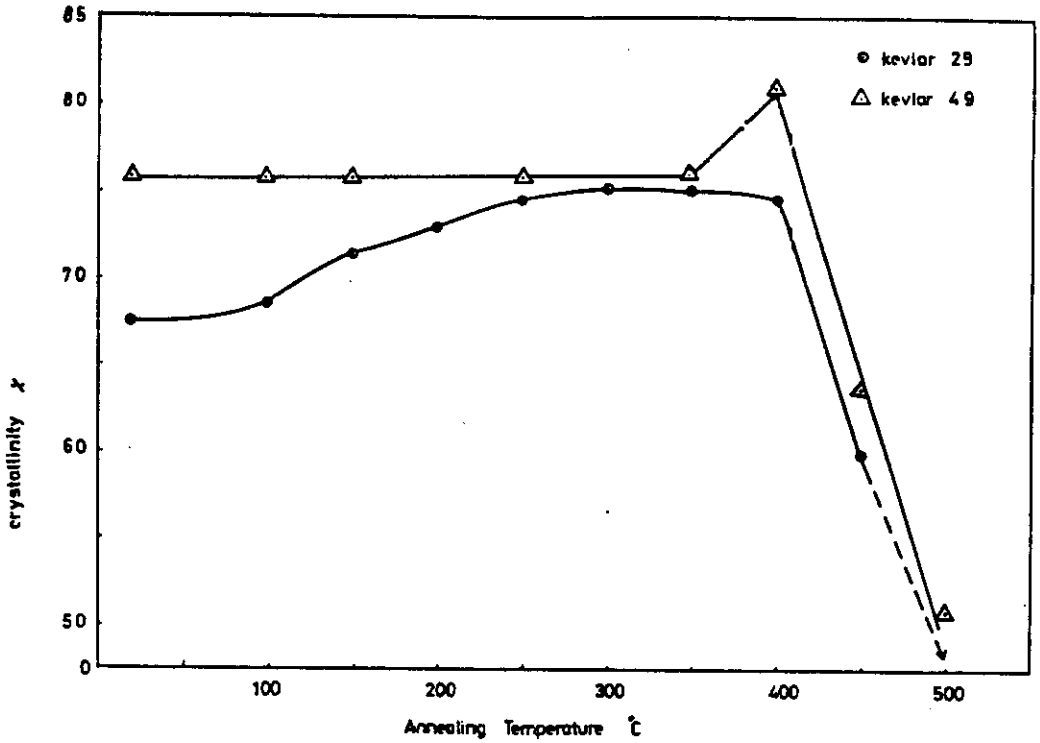

Figure 12

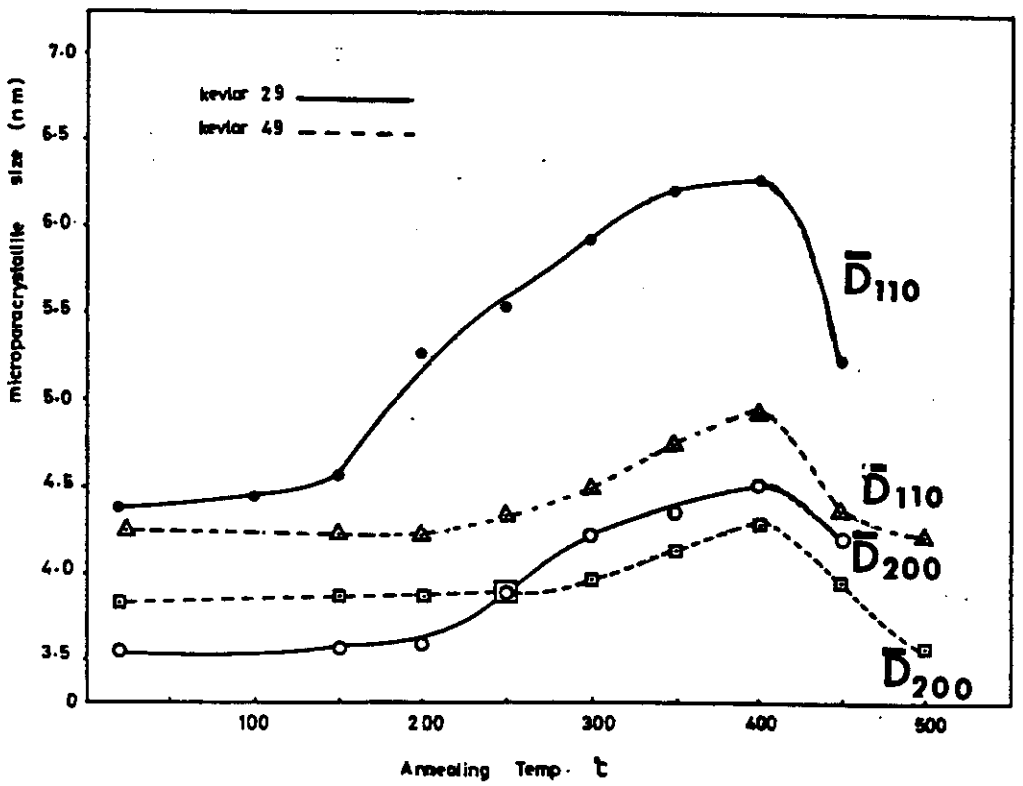

Figure 13

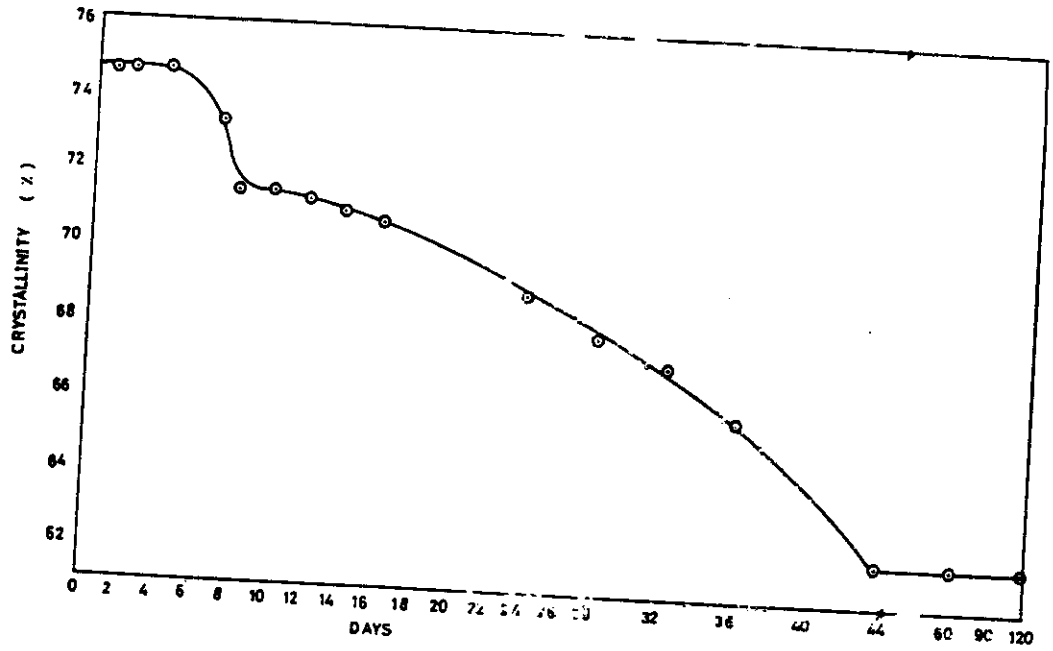

Figure 14

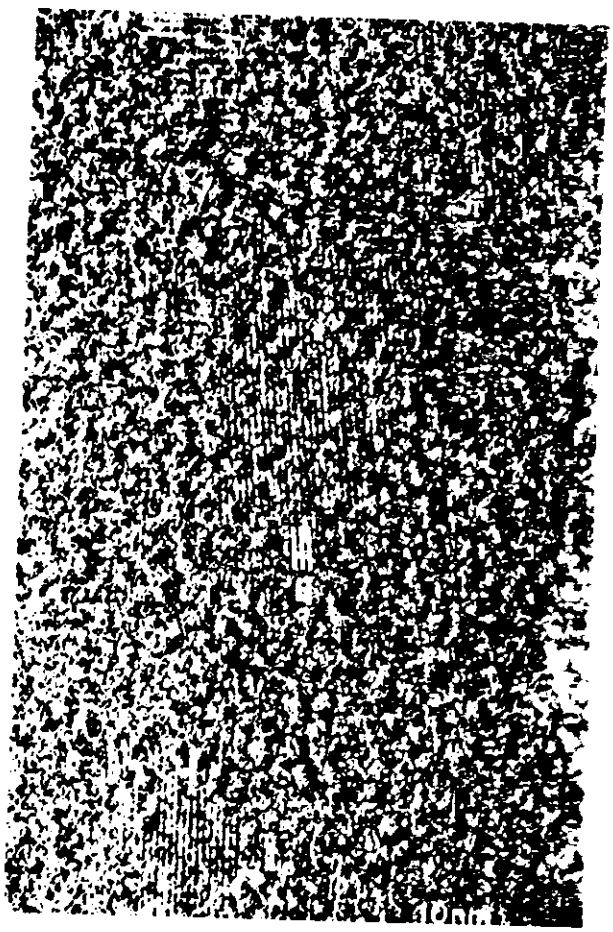

Figure 15

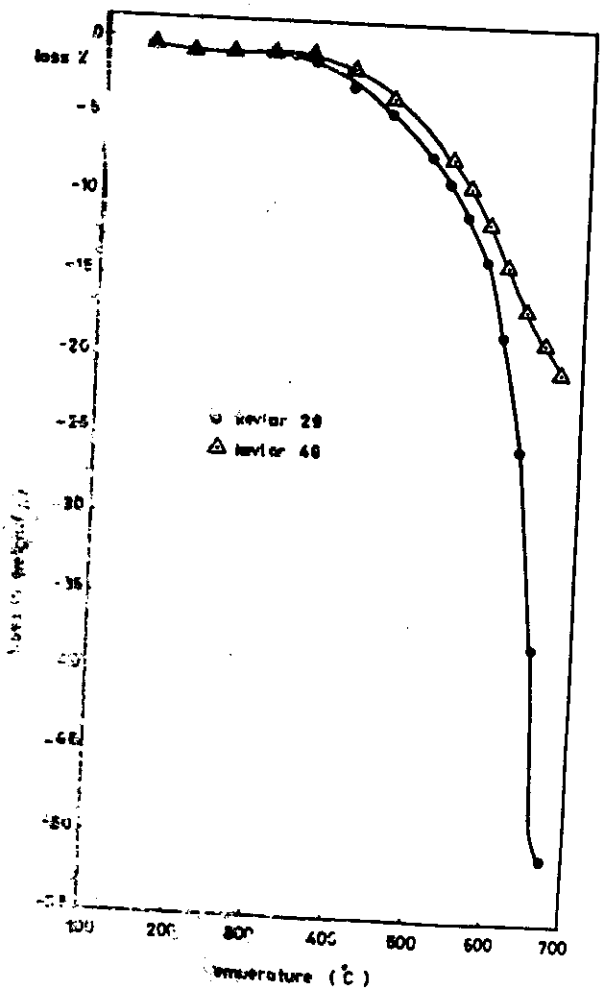

Figure 16

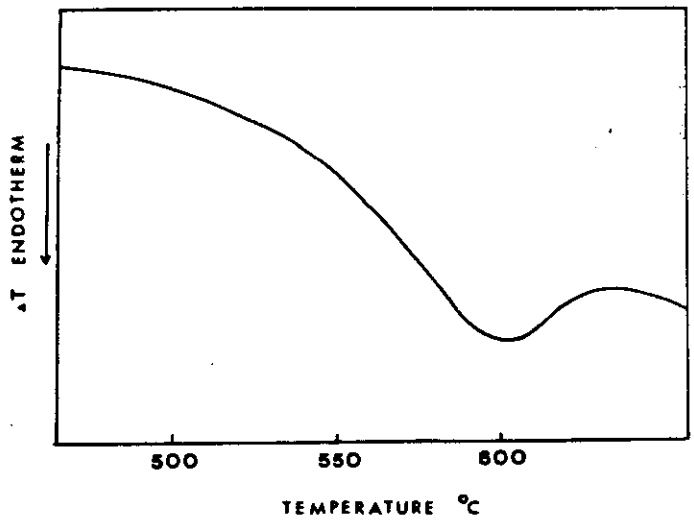

Figure 17

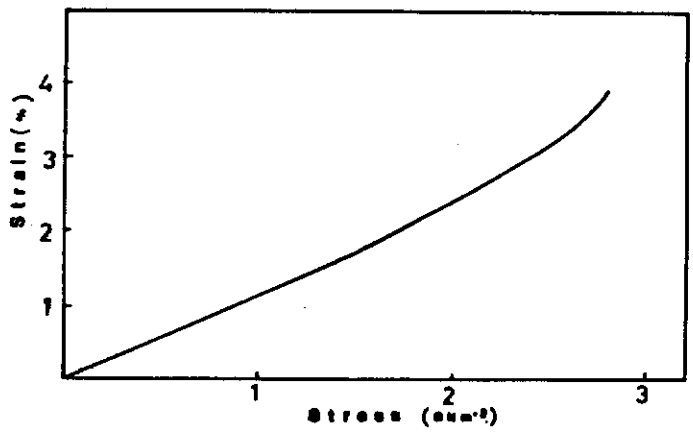

Figure 19

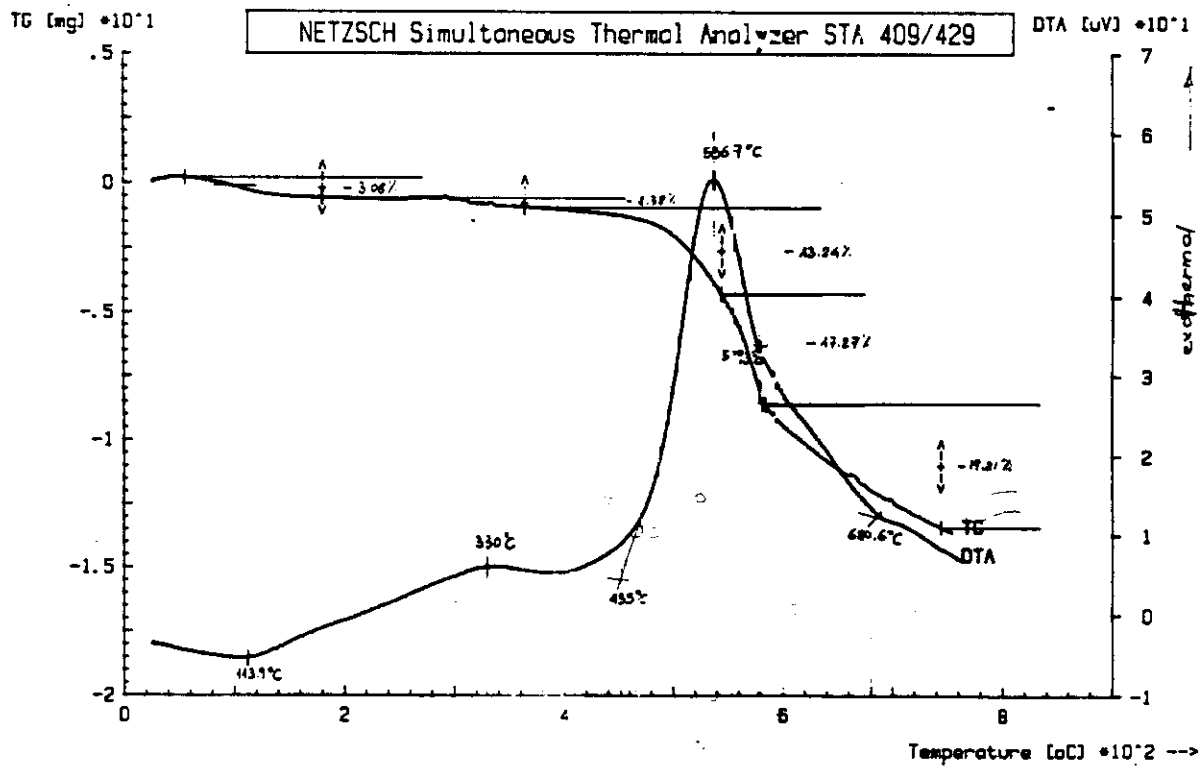

Figure 18

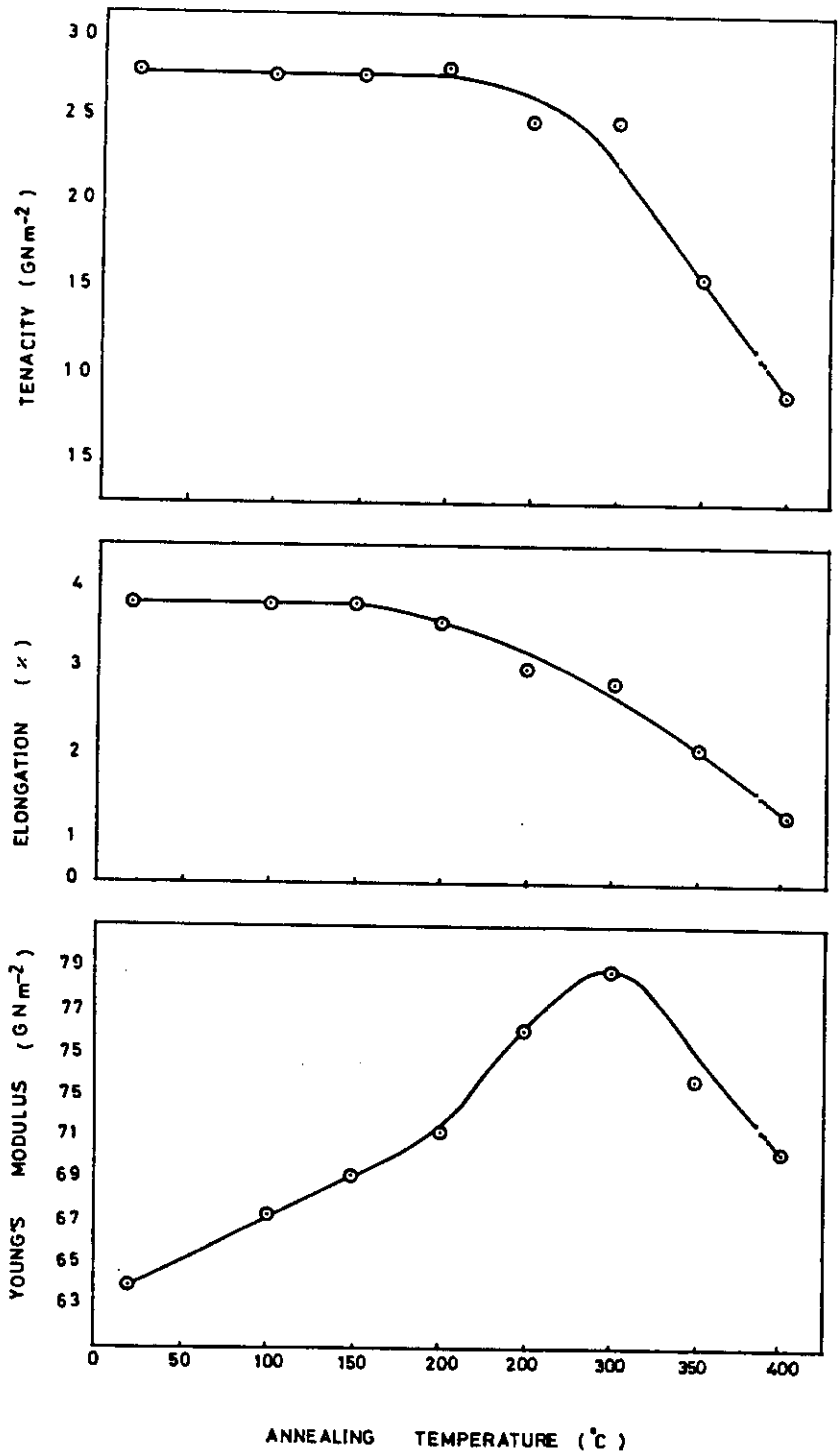
TENACITY (GN m⁻²)
30
25
20
15
10
15
ELONGATION (%)
4
3
2
1
0
YOUNG'S MODULUS (G N m⁻²)
79
77
75
75
71
69
67
65
63
0
50
100
150
200
200
300
350
400
ANNEALING TEMPERATURE (°C)

Figure 20